

# One-shot Weakly-Supervised Segmentation in Medical Images

Anonymous CVPR submission

Paper ID 2249

## Abstract

Deep neural networks usually require accurate and a large number of annotations to achieve outstanding performance in medical image segmentation. One-shot segmentation and weakly-supervised learning are promising research directions that lower labeling effort by learning a new class from only one annotated image and utilizing coarse labels instead, respectively. Previous works usually fail to leverage the anatomical structure and suffer from class imbalance and low contrast problems. Hence, we present an innovative framework for 3D medical image segmentation with one-shot and weakly-supervised settings. Firstly a propagation-reconstruction network is proposed to project scribbles from annotated volume to unlabeled 3D images based on the assumption that anatomical patterns in different human bodies are similar. Then a dual-level feature denoising module is designed to refine the scribbles based on anatomical- and pixel-level features. After expanding the scribbles to pseudo masks, we could train a segmentation model for the new class with the noisy label training strategy. Experiments on one abdomen and one head-and-neck CT dataset show the proposed method obtains significant improvement over the state-of-the-art methods and performs robustly even under severe class imbalance and low contrast.

## 1. Introduction

Precise automatic segmentation of medical images is crucial to various fields, e.g., surgical planning, radiation therapy, and other workflows [28, 55]. In recent years, deep learning-based segmentation algorithms have achieved superior performance with sufficient annotated data. However, collecting medical image segmentation annotations is expensive and time-consuming since it requires domain-specific experts to annotate at the pixel level. Furthermore, the data distribution shift between training and testing sets tends to hurt the generalisability of learned models, further aggravating the scarcity of labeled images [5].

To overcome these challenges, plenty techniques

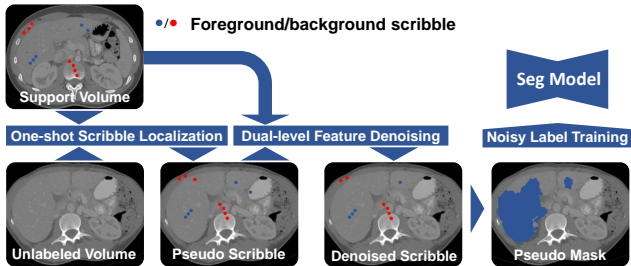


Figure 1. Our method tackles the one-shot medical image segmentation problem by localizing and refining scribbles in unlabeled volumes leveraging anatomical information and training the segmentation model with pseudo masks generated by scribbles using a noisy label training strategy.

have been investigated like semi-supervised- [69], self-supervised- [2, 19, 30], weakly-supervised- [11, 16] and one-shot learning [30, 38, 66]. Among them, one-shot learning is especially appealing because it only requires one annotated example (denoted as support) during the whole training stage and could segment the unlabeled images (denoted as query) in testing stage. Plenty of one-shot segmentation (OSS) methods have been proposed for natural image segmentation tasks [4, 47, 58, 64]. They are mainly based on prototypical networks and mask average pooling to extract class prototypes from feature maps, with the assumption that the prototypes contain enough information to distinguish the boundary around classes. However, different from natural images, medical images often suffer from (1) extreme sample imbalance between small foreground and large background area; (2) low contrast between foreground and surrounding tissues [28]. Therefore, limited prototypes could hardly locate the target organs or separate the contour. Thus current medical image OSS methods based on prototypical networks [38, 45] usually (1) require the range of target organs in one plane be given; (2) failed to segment the boundary in ambiguity area.

Therefore, we propose a novel OSS framework. We argue that previous works directly achieving dense segmentation results based on information from the support set may not be reasonable enough because they could not guaran-

tee the accuracy of the contour voxels or even the correct localization of the target class. Since in most real clinical situations, there are much more unlabeled images than labeled ones [52], it is more feasible to label limited points with high accuracy on unlabeled images, then expand them to formulate a large training set.

More specifically, our method combines one-shot localization (OSL) with weakly-supervised segmentation (WSS), which only requires limited scribble annotations in the support image. First, we propose a propagation-reconstruction network (PRNet) to locate several foreground/background points in unlabeled images. Second, we design a dual-level feature denoising (DFD) method to select the correctly located points with anatomical- and pixel-level features. Then based on these points, we apply a WSS algorithm to achieve pseudo masks for the class-specific segmentation model training. Since the generated masks are not always accurate, we adopt a noisy training strategy to clean the label iteratively and eventually obtain a robust segmentation model.

Our contributions can be summarized as:

- A novel medical image OSS pipeline that combines OSL, WSS, and noisy training strategy to train segmentation models with only one weakly labeled image and several unlabeled images.
- PRNet for propagating scribbles to unlabeled images and DFD method for selecting the correctly located points.
- We demonstrate the effectiveness of our method on one abdomen CT dataset TCIA [8] and one head-and-neck (HaN) dataset StructSeg19. Experiments show that the proposed framework outperforms the state-of-the-art few-shot framework for medical image segmentation largely by an average of 23% on TCIA and 45.4% on StructSeg19 in terms of Dice score.

## 2. Related Work

### 2.1. One-shot Learning:

One-shot learning aims to identify a new category from only one training sample. Most recent works follow the research line of meta-learning, obtaining “generic” knowledge assumed to be shared among the known and unseen classes [12, 13, 49]. These works can be roughly divided into three categories, i.e., the metric-based methods [49, 51, 54], the model-based methods [36, 46], and the optimization-based methods [12, 18].

OSS has achieved progressive success very recently [4, 31, 42, 47, 58, 64]. A major stream of OSS network architecture in natural images is prototypical networks [4, 47], which apply average mask pooling to generate one or multi-feature representations of fore-/background. Following the similar idea, Roy *et al.* [45] first proposes a squeeze and excite architecture specifically for medical images few-shot

segmentation. Tang *et al.* [53] proposes a context relation encoder and a recurrent mask refinement module to refine the segmentation mask iteratively. However, they require the label of other organs around the target one for model training while collecting a large annotated training dataset for medical scans remains elusive due to the shortage of experts, reducing the feasibility of these methods.

To leverage unlabeled data, self-supervised learning (SSL) attracted increasing interest because of its powerful ability in exploring the potential structure of medical image datasets [2, 6, 30, 38, 59, 60]. Ouyang *et al.* [38] proposed a framework exploiting superpixel-based SSL, obtaining representation prototypes unsupervised and eliminating the need for manual annotations, while the model performance largely depends on the selection of superpixels.

Nonetheless, there are two shortages for the prototypical OSS methods mentioned above [38, 45, 53]: 1) they focus on generating prototype representation of support images while neglecting the intrinsic information of the target class itself in query images, e.g., shape, size; 2) they are all 2D-based and need the start and end slice of target organ in one plane be given firstly in inference, which introduces additional supervision information.

Different from them, we expand our training set by localizing support scribbles on unlabeled images then obtaining pseudo masks through WSS algorithms to train the segmentation model. Recently, several works about medical images OSL [30, 59, 60] emerged, which proposed SSL methods for anatomical structure embedding. More specifically, [59, 60] compare the feature cosine similarity between target points and each pixel in query images for localization, while Relative Position Regression (RPR) [30] directly propagating patches to a shared physical 3D coordinate system, thus localizing the target point in a distance regression way. Although great progress has been made, current OSL methods do not have the self-checking mechanism and can not estimate the correctness of localization. Therefore, We extend the propagation networks (PNet) in RPR with an image reconstruction task to extract anatomical- and pixel-level features simultaneously for further filtering.

### 2.2. Weakly Supervised Segmentation

Compared with fully supervised segmentation task which needs time-consuming pixel-wise annotations, WSS requires more flexible annotations like scribbles [32], bounding boxes [24], extreme points [11] and image-level classification labels [1]. Most previous WSS works in natural images achieve impressive performance by refining the CAMs [68] generated by the image classifier to approximate the segmentation mask [1, 17, 20]. WSS also attracts great interest in the medical image analysis community due to its potential of reducing data labeling require-

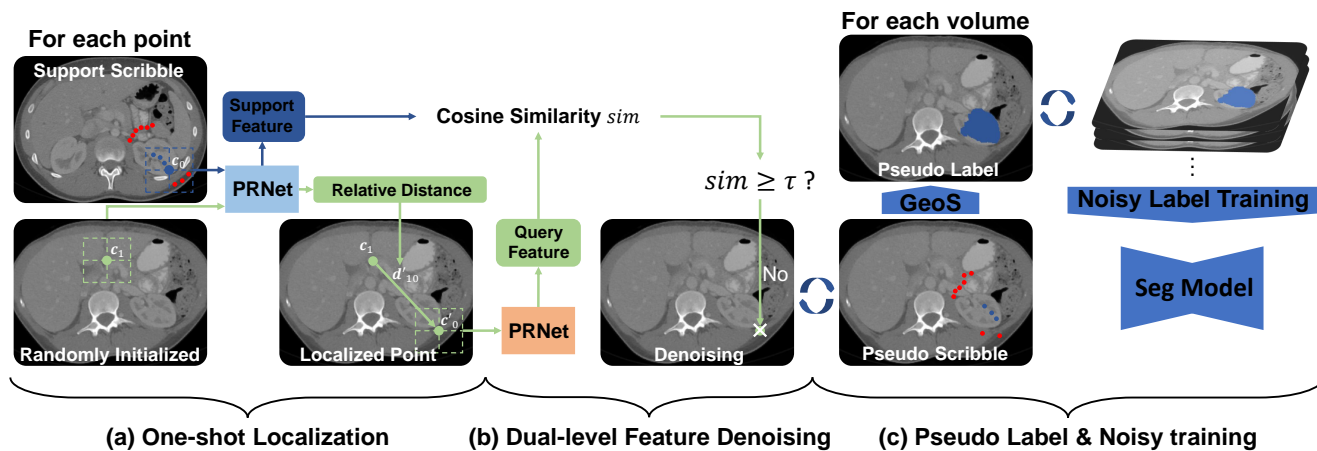


Figure 2. An overview of the proposed method. (a) One-shot scribble localization network for propagating the scribbles of support volume to the unlabeled volume; (b) Dual-level feature denoising to refine the scribbles generated by OSL; (c) Generate pseudo masks with the scribbles GeoS method to train the segmentation task.

ments, where the bounding boxes [22, 23, 41] and scribbles [9, 29, 57] are the most commonly used annotation type. Among all these methods, geodesic image segmentation (GeoS), which encodes spatial regularization and contrast sensitivity, has shown superior performance [11, 29, 57]. Therefore, we adopt GeoS to form the pseudo masks used for supervision. However, generated masks may be inaccurate in practice, so we investigate noisy label learning to achieve better performance.

### 2.3. Learning from Noisy Labels

Many studies have shown that label noise can significantly impact the performance of deep learning models [3, 15, 21, 43, 48, 56, 63]. Existing studies dealing with label noise could be organized under six categories: 1) Label cleaning and pre-processing [37, 40]; 2) Network architecture [10, 50]; 3) Loss functions [14, 33]; 4) Data reweighting [26, 43]; 5) Data and label consistency [27, 62]; 6) Training procedures [35, 67].

Karimi *et al.* [21] investigates the performance of different noisy-label learning approaches in approximate fetal brain segmentation generated by registration, intensity thresholding, and level set, which shares a similar situation with this propagate when training the segmentation model from pseudo masks. The experiment results show that the iterative label cleaning strategy achieves the best performance. Following this conclusion, we utilize a state-of-the-art cleaning training method [65] that iteratively corrects labels with predicted probabilities above a decreasing threshold.

## 3. Method

In this section, we first introduce the problem setting and an overview of our framework. Then we elaborate details

of it. To be simplified, we focus on binary segmentation, which could be easily extended to multi-classes.

### 3.1. Problem Formulation

Let  $f_\theta$  be a CNN parametrized by the weights  $\theta$  that predicts the probability of being foreground for each voxel.  $\{X_u\}$  represents a set of unlabeled grayscale 3D medical image scans, and  $[X_s, Y_s]$  represents a support volume with its scribble annotation. We focus on the challenging setting of OSS that trains  $f_\theta$  one support 3D image scans  $[X_s, Y_s]$  and a set of unlabeled cases  $\{X_u\}$ .

As shown in Fig. 2, our approach contains three parts:

1) For each point  $c_0$  in the support scribble and a randomly selected point  $c_1$  in the unlabeled volume, PRNet takes the patches around them respectively to predict their relative distance  $d'_{10}$  and keep the support feature vectors. Then we move  $c_1$  to  $c'_0$  with  $d_{10}$  as a temporally located point.

2) We crop the patch around  $c'_0$  to PRNet and get the query feature vectors. Then we calculate the cosine similarity  $sim$  between support and query feature vectors. If  $sim$  surpasses  $\tau$ , the  $c'_0$  would be kept, otherwise be deleted. We go through all the points in scribble and achieve the final propagated results.

3) With the pseudo scribbles, we apply geodesic distance-based weakly supervised segmentation method [9, 57] generating pseudo masks for each subject then train a segmentation model.

### 3.2. Scribble Localization

Because a scribble could be viewed as a set of adjacent points, it is easy to obtain their counterparts in the query volume based on one-shot landmark localization frameworks [30, 59, 60]. However, due to the large variance

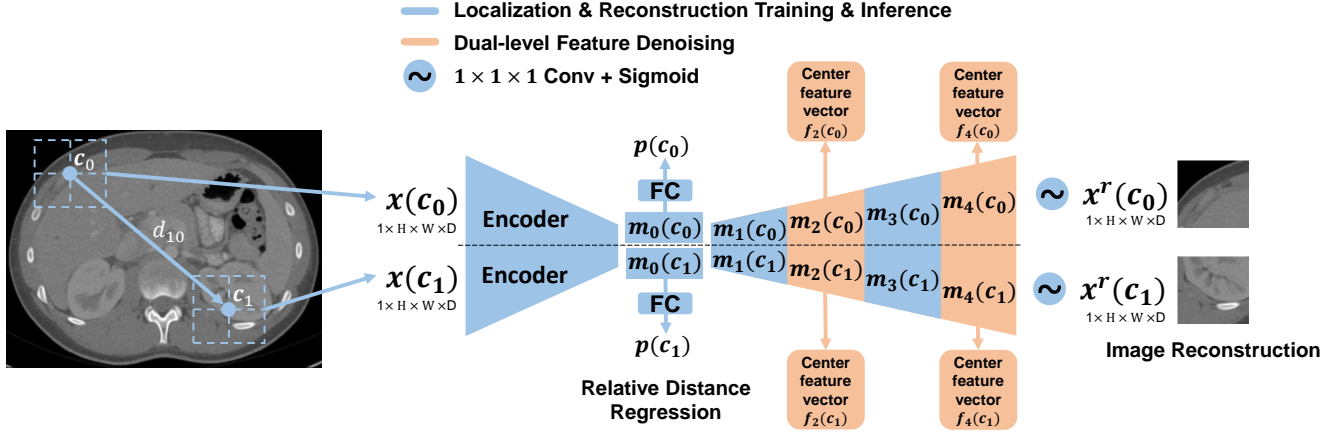


Figure 3. PRNet is composed of three parts: an encoder, fully connected layers and a decoder. The encoder contains four blocks of convolutions and  $2 \times 2 \times 2$  downsampling while the decoder contains four blocks of convolutions and  $2 \times 2 \times 2$  upsampling.  $m_i$  represents the feature map after  $i$  times upsampling. We train PRNet with relative distance regression and image reconstruction: with two randomly selected points  $c_0$  and  $c_1$  from the same volume, we crop patches  $x(c_0)$ ,  $x(c_1)$  and pass them into PRNet to get their anatomical coordinate predictions  $p(c_0)$ ,  $p(c_1)$  and reconstruction results  $x^r(c_0)$ ,  $x^r(c_1)$ . Then we calculate the loss with Eq. 3. After training, we apply PRNet to propagate every point from support scribbles to query volumes. And to filter out correctly located points, we use DFD to the center corresponding feature vectors from  $m_2$  and  $m_4$  of the support point and the located point.

among individuals, the located points may not be accurate enough and fall into the wrong areas, decreasing the segmentation performance. To resolve this issue and refine the noisy propagation, we propose a self-supervised feature similarity-based method.

RPR [30] propagates the medical scan patch into a shared 3D coordinate system, representing its anatomical position in the human body. We further assume that the information a medical scan patch holds could be disentangled as anatomical-level position (where the patch is) and the pixel-level representation (what kind of tissue the patch contains). Thus for a correctly located point, its features should be similar to the support point on both two levels, and the key falls in extracting the anatomical- and pixel-level feature from unlabeled data.

Thus, we extend RPR with an image reconstruction task to extract pixel-level features simultaneously. More specifically, we add a decoder in the PNet of RPR for image reconstruction and design a propagation-reconstruction network (PRNet). The structure of PRNet is shown in Fig. 3, in which  $m_i$  means the feature map after  $i$  times upsampling. We train the PRNet with two SSL tasks: relative distance regression and image reconstruction.

During the training stage, we randomly select a volume  $X_u$  from unlabeled set and two points  $c_0(c_0^z, c_0^x, c_0^y)$ ,  $c_1(c_1^z, c_1^x, c_1^y)$  from it. Then we crop two patches  $x(c_0)$ ,  $x(c_1)$  around  $c_0$ ,  $c_1$  with fixed size  $H \times W \times D$ , respectively. Assuming the pixel spacing of  $X_u$  is  $e \in R^3$ , the ground truth offset  $d_{10}$  from  $x(c_0)$  to

$x(c_1)$  in the physical space is denoted as:

$$d_{10} = (c_1 - c_0) \circ e \quad (1)$$

where  $\circ$  represents the element-wise product.

We send  $x(c_0)$ ,  $x(c_1)$  to PRNet and obtain 4 items: (1) anatomical 3D coordinate predictions  $p(c_0)$ ,  $p(c_1)$ ; (2) image reconstruction  $x^r(c_0)$ ,  $x^r(c_1)$ ; (3) anatomical-level feature vectors  $f_2(c_0)$ ,  $f_2(c_1)$  from the center of feature maps  $m_2(c_0)$ ,  $m_2(c_1)$ ; (4) pixel-level feature vectors  $f_4(c_0)$ ,  $f_4(c_1)$  from the center of feature maps  $m_4(c_0)$ ,  $m_4(c_1)$ . The last two items will be used for judging the correctness of located points in Sec. 3.2. Then the predicted offset  $d'_{10}$  from  $c_1$  to  $c_0$  is obtained as:

$$d'_{10} = r \cdot \tanh(p(c_0) - p(c_1)) \quad (2)$$

where the hyperbolic tangent function  $\tanh$  and the hyper-parameter  $r$  together control the upper and lower bound of dq, which is set to cover the largest possible offset. Finally, we apply the mean square error (MSE) to measure the relative distance and reconstruction loss:

$$\begin{aligned} L_{ssl} &= L_{dis} + L_{rec} \\ L_{dis} &= \frac{1}{3} \|d_{10} - d'_{10}\|_2^2 \\ L_{rec} &= \frac{1}{N} (\|x(c_0) - x^r(c_0)\|_2^2 + \|x(c_1) - x^r(c_1)\|_2^2) \end{aligned} \quad (3)$$

where  $N = H \times W \times D$  is the number of total voxels of the patch.



After self-supervised training, the network can be directly used for localization on any landmark contained in the training dataset.

Given a support volume  $[X_s, Y_s]$ , our mission is localizing every point in  $Y_s = \{y(c_0), y(c_1), \dots, y(c_i), \dots\}$  on unlabeled volume set  $\{X_u\}$ , in which  $y(c_i)$  represents the label of point  $c_i$ .

We start from point  $c_0$  and traverse around the scribble. By the same token with training stage, we first crop patch  $x(c_0)$  around  $c_0$  from  $X_s$  and pass it through PRNet to achieve the corresponding anatomical coordinate  $p(c_0)$ , feature vectors  $f_2(c_0)$  and  $f_4(c_0)$ . Then given an unlabeled image  $X_u$ , we randomly crop a patch  $x(c_1)$  with center point  $c_1$  to get  $p(c_1)$ ,  $f_2(c_1)$  and  $f_4(c_1)$ . The relative distance  $d'_{10}$  from  $c_1$  to  $c_0$  is obtained with Eq. (2). Thus the located point  $c'_0$  can be obtained by moving  $c_1$  with  $d'_{10}$ :

$$c'_0 = c_1 + d'_{10} \quad (4)$$

### 3.3. Dual-level Feature Denoising

To validate the correctness of  $c'_0$ , we propose dual-level feature denoising (DFD): we first crop patch  $x(c'_0)$  from  $X_u$  and feed it into PRNet, getting corresponding two level feature vectors  $f_2(c'_0)$  and  $f_4(c'_0)$ . The theoretical reasoning and experiments in [7] indicate a quadratic relation between the label noise ratio in the training data and test error. Consequently, we focus on improving the precision of located points rather than the total number.

A key observation of this research is that the feature vectors of located point and the support point are highly comparable in the lower level feature maps near the fully connected layers, i.e.,  $m_0(c_0), m_0(c'_0)$  and  $m_1(c_0), m_1(c'_0)$ . Because the predicted anatomical coordinate  $p(c_0), p(c'_0)$  are fully depended on the 0 level feature map  $m_0(c_0), m_0(c'_0)$ .  $p(c_0) \approx p(c'_0)$  implies the equivalence of  $m_0(c_0)$  and  $m_0(c'_0)$ . The low-level feature maps in the decoder hold anatomical information, and the high-level feature maps represent pixel-level information.

Therefore, we select  $f_2(c_0), f_2(c'_0)$  in  $m_2(c_0), m_2(c'_0)$  and  $f_4(c_0), f_4(c'_0)$  in  $m_4(c_0), m_4(c'_0)$  from the support and query volumes, and calculate the cosine similarity of these two level features, then multiply them to get variable  $sim$ , quantifying the similarity of  $c_0$  and  $c'_0$  in anatomical and pixel-level simultaneously:

$$sim = \cos(f_2(c_0), f_2(c'_0)) \cdot \cos(f_4(c_0), f_4(c'_0)) \quad (5)$$

$c'_0$  will be labeled as class  $y(c_0)$  if  $sim > \tau$ , otherwise be discarded. Eventually, we obtain the scribble propagation  $Y_u$  for each  $X_u$ . In the inference stage, the same process could be applied to get the pseudo scribble  $Y_q$  from the given query volume  $X_q$ .

### 3.4. Pseudo Mask Generation and Noisy Label Training

Based on the pseudo scribble, we now propose to create our trainable samples in unlabeled set  $\{X_u, L_u\}$  by generating pseudo masks  $L_u$  with GeoS [9, 57] for each  $[X_u, Y_u]$ .  $f_\theta$  is based on a 3D UNet [44] and we use the sum of cross entropy and dice loss [34] for supervision, which is commonly used in medical image segmentation.

The experiments in Karimi *et al.* [21] suggest that iterative label cleaning method achieves the best performance for the pseudo mask training. According to its conclusion, we adopt the state-of-the-art label correction algorithm PLC (Progressive Label Correction) [61] that iteratively corrects labels and refines the model  $f_\theta$  for training. For each point  $c_i$ , if the prediction of  $f_\theta$  is different from its pseudo mask  $l(c_i)$  and its confidence is above the threshold,  $f_\theta(c_i) > \delta$ , the label  $l(c_i)$  is flipped to the prediction of  $f_\theta$ . We repeatedly correct masks and improve the network until it converges.

## 4. Experiments

### 4.1. Dataset and Evaluate Metric

To demonstrate the generalization of our method, we perform evaluation under two highly different CT datasets: abdomen organs segmentation and HaN organs segmentation:

- The Cancer Image Archive (TCIA) Pancreas CT dataset [8] contains 43 patients with various abdomen tumors. In practice, we test our method on 3 organs: liver, spleen and left liver<sup>1</sup>. They make up about **8.5%** of the total volume.

- Automatic Structure Segmentation for Radiotherapy Planning Challenge 2019<sup>2</sup> (StructSeg19) task 1 contains 50 HaN CT scans from nasopharynx cancer patients. We test our method on 3 organs: brain stem, right/left parotid glands (right/left PG), which account for **0.1%** voxels in total.

For both two datasets, we use 60% of data for training, 20% for validation, and the remaining 20% are used for testing. We use the same evaluation metric Dice score as in previous works [38, 66]. Dice score (0-1, 0: mismatch; 1: perfectly match) measures the overlap of the prediction  $M$  and ground truth  $G$ , and is defined as:

$$Dice(M, G) = \frac{2|M \cap G|}{|M| + |G|} \quad (6)$$

### 4.2. Implementation Details

The whole framework is implemented with Pytorch [39] and public available<sup>3</sup>. Our model is trained with a NVIDIA GTX 1080 Ti GPU. The Adam optimizer [25] is used for training with batch size 8, initial learning rate  $10^{-3}$  with

<sup>1</sup><https://zenodo.org/record/1169361#.YXUabRrP2Uk>

<sup>2</sup><https://structseg2019.grand-challenge.org/Home/>

<sup>3</sup>[https://anonymous.4open.science/r/OneShot\\_WeaklySeg-CFBC](https://anonymous.4open.science/r/OneShot_WeaklySeg-CFBC)

Table 1. Dice score (%) comparison in testing set.

Method	Manual Local.?	TCIA				StructSeg19			
		Spleen	Left Kidney	Liver	Mean	Brain Stem	Left PG	Right PG	Mean
SE-Net [45]	✓	32.9±10.6	30.5±16.2	54.0±6.9	39.1±9.1	4.6±1.8	2.2±0.5	2.0±0.5	2.9±0.7
SSL-ALPNet [38]	✓	57.5±12.0	63.9±10.6	75.6±4.4	65.7±6.4	23.9±4.0	13.6±4.4	20.0±6.5	19.1±3.9
Aug [66]	✗	36.3±19.0	16.4±25.8	81.2±14.8	44.6±18.4	55.6±10.6	30.2±13.2	33.8±15.7	39.9±12.4
PRNet (ours)	✗	<b>84.9±12.0</b>	<b>90.9±4.1</b>	<b>90.3±3.6</b>	<b>88.7±4.2</b>	<b>75.2±3.4</b>	<b>74.6±3.3</b>	<b>76.0±2.8</b>	<b>75.3±3.2</b>
Fully Supervised	✗	90.2±14	95.0±1.6	93.9±4.8	93.0±6.3	82.9±3.6	85.8±2.1	84.9±4.0	84.9±3.5

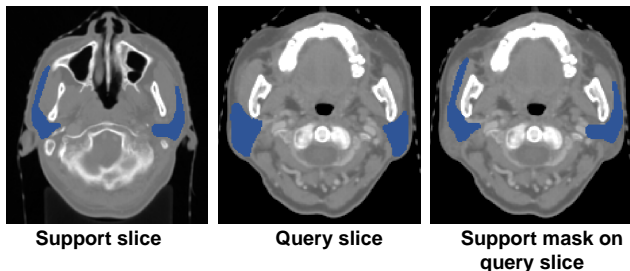


Figure 4. Visualization example of low intersection of parotid glands between support and query slices in StructSeg19.

a stepping decay rate of 0.9 per 10 epochs and 150 epochs totally. Along  $zxy$  plane, TCIA and StructSeg19 images are resampled to  $3 \times 1 \times 1 \text{ mm}^3$  and  $1 \times 1 \times 1 \text{ mm}^3$ , respectively. Fixed patch size  $48 \times 128 \times 128$  voxels is applied for PRNet training in both datasets. We set  $\tau = 0.5$  for DFD.  $\delta$  is set as 0.95 for PLC at beginning and times 0.99 every epoch till it reaches 0.85.

We focus on the task of segmentation using one volume labeled with scribbles. We select the first subject in training data as support volume and draw the scribbles manually, then apply PRNet propagating them on the remaining ones to generate pseudo scribbles and use GeoS to obtain the pseudo masks. We crop the target organs around the boundary of pseudo masks for training to reduce the class imbalance between foreground and background. We compare the performance of models trained on pseudo masks generated by original/noise-reduction pseudo scribbles in Sec. 4.4.

#### 4.3. Comparison with State-of-the-art Methods

Table 1 shows the comparisons of our method with 3 open-source OSL methods: SE-Net [45], SSL-ALPNet [38] and DataAug [66], a data augmentation methods for synthesizing labeled medical image. For SE-Net and SSL-ALPNet, we adopt the same setting in their works, cropping the query volume among the bottom and top slice of the target organ first then dividing it into 3 equally-spaced chunks to be segmented with corresponding support slices. We also train a fully-supervised segmentation 3D UNet that

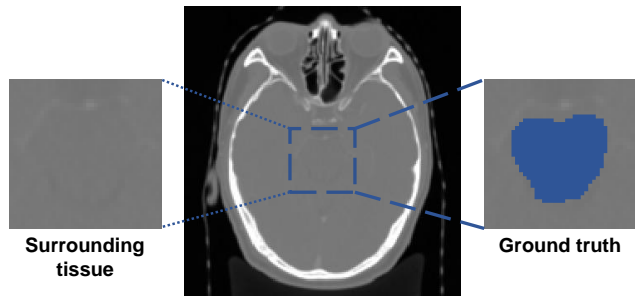
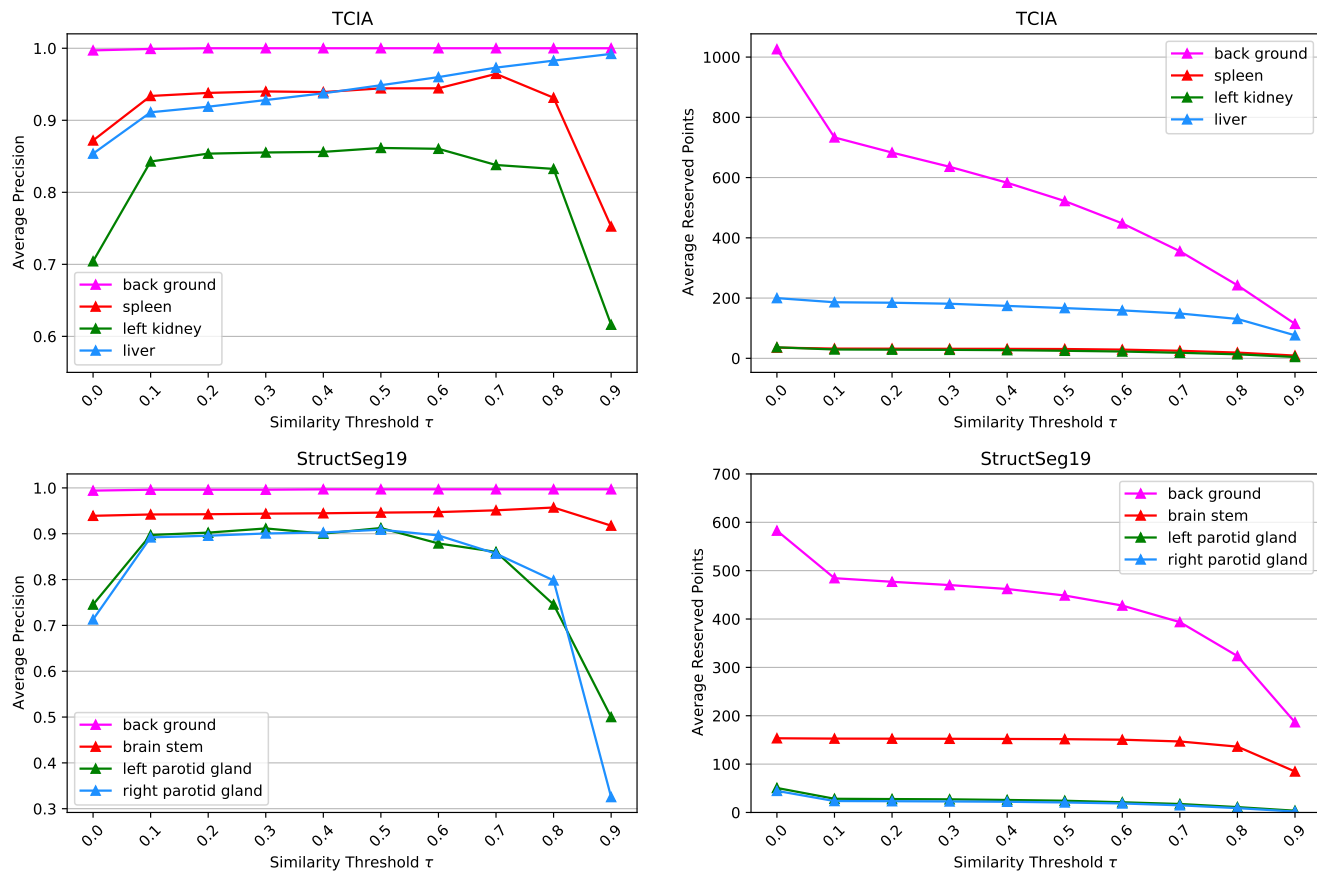


Figure 5. Visualization example of low contrast between brain stem and surrounding tissue in StructSeg19.

uses ground truth labels for all examples in our training dataset to serve as the upper bound.

Without being indicated the range of slices where the organ lies, our proposed PRNet outperforms others largely, especially in StructSeg19. There are mainly 2 reasons: (1) SE-Net passes the support set through the conditioner arm, whose information is conveyed to the segmenter arm via interaction blocks. It assumes that the target organ in the support slice is roughly aligned with the one in the query. However, due to the limited volume size of organs in HaN, even slight intersecting pixels of target organs between support and query slices caused by small variance among patients could make the above assumption unsatisfied. Fig. 4 presents an visualization example of parotid glands. It could be observed that the propagation of the support mask on query slice has a small overlap with the ground truth; (2) SSL-ALPNet utilizes a self-supervised superpixel segmentation task then uses the learned representations to segment new classes without fine-tuning. However, as shown in Fig. 5, the contrast of organs, e.g., brain stem in StructSeg19 with surrounding tissue, is extremely low even after normalization, which is vital to SSL-ALPNet because it could hardly select superpixels distinguishing the boundary of target organs during training time. In contrast, our method first locates fore-/background scribbles in query volumes, thus is not sensitive to the extreme sample imbalance and low contrast.

Figure 6. Average precision and the number of reserved points under different  $\tau$  in validation set.Table 2. Ablation study (in Dice score) on  $\tau$  values in testing set.

$\tau$	TCIA				StructSeg19			
	Spleen	Left Kidney	Liver	Mean	Brain Stem	Left PG	Right PG	Mean
0.0	69.6 $\pm$ 17.3	51.6 $\pm$ 27.5	82.9 $\pm$ 5.7	68.0 $\pm$ 13.2	<b>74.4<math>\pm</math>2.1</b>	53.3 $\pm$ 24.0	51.4 $\pm$ 23.1	59.7 $\pm$ 14.6
0.5	<b>81.1<math>\pm</math>12.6</b>	<b>70.0<math>\pm</math>23.4</b>	<b>83.2<math>\pm</math>5.5</b>	<b>78.1<math>\pm</math>11.6</b>	74.0 $\pm$ 2.0	<b>64.7<math>\pm</math>11.3</b>	<b>65.9<math>\pm</math>15.0</b>	<b>68.2<math>\pm</math>7.7</b>
0.9	43.6 $\pm$ 35.6	21.9 $\pm$ 25.1	70.1 $\pm$ 10.9	45.2 $\pm$ 16.1	67.3 $\pm$ 6.9	9.2 $\pm$ 23.8	19.5 $\pm$ 27.7	32.0 $\pm$ 16.1

#### 4.4. Ablation Study

**Effect of DFD** To verify the contribution of DFD, we conduct experiments at two stages: (1) scribble propagation; (2) pseudo masks generation with original/denoised scribbles.

First, to confirm the denoising ability of DFD and select the appropriate  $\tau$ , we gradually increase  $\tau$  from 0 to 0.9 and evaluate the results in the validation set. Fig. 6 shows the class-specific average precision and the number of reserved points per volume before and after denoising. For most classes, even be filtered with the lowest level ( $\tau = 0.1$ ), their propagation precision would increase largely. For example, left/right parotid glands with  $\tau = 0.1$  outperform the original results ( $\tau = 0$ ) by an average precision score



Figure 7. Visualization example of the denoised scribble. After denoising, spleen scribble propagation (blue) on the top right corner has no intersection with the background area, while the remaining correctly located spleen and background scribbles (red) are reserved.

around 20%. A visual comparison example is presented in Fig. 7, in which DFD successfully deletes the incorrectly located spleen scribble (blue) while reserving others.

Table 3. Ablation study (in Dice score) on model training in testing set.

Method	Training	TCIA			Mean	Brain Stem	StructSeg19		Mean
		Spleen	Left Kidney	Liver			Left PG	Right PG	
RDR+GeoS	✗	81.1±12.6	70.0±23.4	83.2±5.5	78.1±11.6	74.0±2.0	64.7±11.3	65.9±15.0	68.2±7.7
RDR+GeoS	✓	<b>85.3±11.5</b>	73.2±23.7	87.3±5.0	81.9±11.2	73.4±5.1	74.1±2.0	<b>77.0±2.1</b>	74.8±2.2
RDR+GeoS+PLC	✓	84.9±12.0	<b>90.9±4.1</b>	<b>90.3±3.6</b>	<b>88.7±4.2</b>	<b>75.2±3.4</b>	<b>74.6±3.3</b>	76.0±2.8	<b>75.3±3.2</b>

However, when  $\tau$  reaches 0.9, it witnesses a steep decrease in both average precision and reserved points for almost all classes. The reason is that for some subjects,  $\tau$  with such a high value may remove all propagated points, leading to their precision and the number of reserved points equal to 0. Therefore, to balance the precision and the number of reserved points, we set  $\tau = 0.5$ .

Another interesting phenomenon is that for both datasets, the precision of background scribbles remains approximately equal to 1. It's mainly because of the extreme imbalance between background and foreground pixels. The background part takes up nearly 91.5% in TCIA and 99.9% in StructSeg19 thus the propagated points are highly likely to fall into the background area.

Second, we explore how the noise reduction affects the accuracy of pseudo masks. We compare the pseudo masks generated by GeoS from scribbles filtered with different  $\tau = 0, 0.5, 0.9$ . As shown in Table 2, the  $\tau = 0.5$  in subsequent experiments brings around 10% improvement than original results in both datasets. As expected in Sec. 3.2, improving the precision of located points rather than the total number brings higher pseudo masks accuracy. The results in Table 2 show that our method could yield competitive performance even without further training.

**Effect of Noisy Training** To show the necessity and advantages of the noisy training, we conduct experiments training  $f_\theta$  with and without PLC, shown in Table 3. From the table, we can observe that  $f_\theta$  brings a 3.8% and 6.6% improvement in TCIA and StructSeg19 compared to the pseudo masks. This implies that even without any specific setting, deep CNNs are robust to strong label noise. With iterative label cleaning, PLC brings an extra 6.8% improvement in TCIA and 0.5% in StructSeg19.

Fig. 8 shows segmentation examples under different settings. It could be noted that even with very sparse support annotations, our training model could yield precise results.

## 5. Conclusion and Discussion

In this work, we present a novel one-shot medical image segmentation framework, which incorporates one-shot localization and weakly-supervised segmentation. Given one image labeled with scribbles and plenty of unlabeled volumes, the proposed method first locates support scribbles on each image, then filters them with proposed dual-level feature denoising and applies WSS algorithms to build a

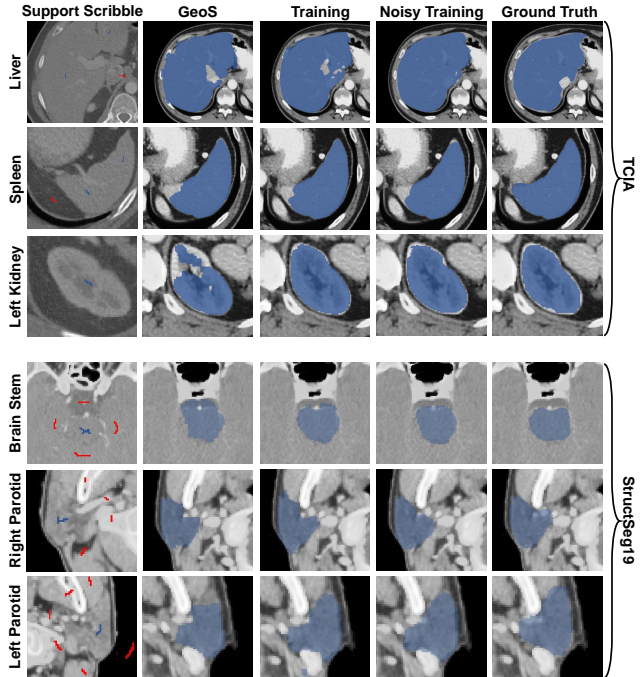


Figure 8. Examples of predictions under different stages.

large training set. We use the generated masks to train a supervised segmentation model with noisy training algorithms for every class. Experiments on two public datasets demonstrate that without manual localization, our method outperforms existing OSS models largely and could perform robustly even under the extreme sample imbalance. What's more, our method could be easily promoted with future improvement in WSS algorithms and noisy training algorithms. And the proposed DFD could be used for judging the correctness of the results in any landmark or organ localization tasks.

## 6. Limitations

Since the proposed PRNet is based on the assumption that different people share similar anatomical structures, it may not yield satisfying results under extreme situations. For example, our model trained on the scans of adults may fail in locating and segmenting organs on scans of infants. But it could be resolved by fine-tuning the model with several unlabeled target scans.



## References

- [1] Jiwoon Ahn and Suha Kwak. Learning pixel-level semantic affinity with image-level supervision for weakly supervised semantic segmentation. In *Proceedings of the IEEE Conference on Computer Vision and Pattern Recognition*, pages 4981–4990, 2018. 2
- [2] Wenjia Bai, Chen Chen, Giacomo Tarroni, Jinming Duan, Florian Guitton, Steffen E Petersen, Yike Guo, Paul M Matthews, and Daniel Rueckert. Self-supervised learning for cardiac mr image segmentation by anatomical position prediction. In *International Conference on Medical Image Computing and Computer-Assisted Intervention*, pages 541–549. Springer, 2019. 1, 2
- [3] David Berthelot, Nicholas Carlini, Ian Goodfellow, Nicolas Papernot, Avital Oliver, and Colin Raffel. Mixmatch: A holistic approach to semi-supervised learning. *arXiv preprint arXiv:1905.02249*, 2019. 3
- [4] Sergi Caelles, Kevis-Kokitsi Maninis, Jordi Pont-Tuset, Laura Leal-Taixé, Daniel Cremers, and Luc Van Gool. One-shot video object segmentation. In *Proceedings of the IEEE conference on computer vision and pattern recognition*, pages 221–230, 2017. 1, 2
- [5] Daniel C Castro, Ian Walker, and Ben Glocker. Causality matters in medical imaging. *Nature Communications*, 11(1):1–10, 2020. 1
- [6] Krishna Chaitanya, Ertunc Erdil, Neerav Karani, and Ender Konukoglu. Contrastive learning of global and local features for medical image segmentation with limited annotations. *arXiv preprint arXiv:2006.10511*, 2020. 2
- [7] Pengfei Chen, Ben Ben Liao, Guangyong Chen, and Shengyu Zhang. Understanding and utilizing deep neural networks trained with noisy labels. In *International Conference on Machine Learning*, pages 1062–1070. PMLR, 2019. 5
- [8] Kenneth Clark, Bruce Vendt, Kirk Smith, John Freymann, Justin Kirby, Paul Koppel, Stephen Moore, Stanley Phillips, David Maffitt, Michael Pringle, et al. The cancer imaging archive (tcia): maintaining and operating a public information repository. *Journal of digital imaging*, 26(6):1045–1057, 2013. 2, 5
- [9] Antonio Criminisi, Toby Sharp, and Andrew Blake. Geos: Geodesic image segmentation. In *European Conference on Computer Vision*, pages 99–112. Springer, 2008. 3, 5
- [10] Yair Dgani, Hayit Greenspan, and Jacob Goldberger. Training a neural network based on unreliable human annotation of medical images. In *2018 IEEE 15th International Symposium on Biomedical Imaging (ISBI 2018)*, pages 39–42. IEEE, 2018. 3
- [11] Reuben Dorent, Samuel Joutard, Jonathan Shapey, Aaron Kujawa, Marc Modat, Sebastien Ourselin, and Tom Vercauteren. Inter extreme points geodesics for weakly supervised segmentation. In *Medical Image Computing and Computer Assisted Intervention—MICCAI 2021*. 2021. 1, 2, 3
- [12] Chelsea Finn, Pieter Abbeel, and Sergey Levine. Model-agnostic meta-learning for fast adaptation of deep networks. In *International Conference on Machine Learning*, pages 1126–1135. PMLR, 2017. 2
- [13] Chelsea Finn, Kelvin Xu, and Sergey Levine. Probabilistic model-agnostic meta-learning. *arXiv preprint arXiv:1806.02817*, 2018. 2
- [14] Aritra Ghosh, Himanshu Kumar, and PS Sastry. Robust loss functions under label noise for deep neural networks. In *Proceedings of the AAAI Conference on Artificial Intelligence*, volume 31, 2017. 3
- [15] Bo Han, Quanming Yao, Xingrui Yu, Gang Niu, Miao Xu, Weihua Hu, Ivor Tsang, and Masashi Sugiyama. Co-teaching: Robust training of deep neural networks with extremely noisy labels. *arXiv preprint arXiv:1804.06872*, 2018. 3
- [16] Yipeng Hu, Marc Modat, Eli Gibson, Wenqi Li, Nooshin Ghavami, Ester Bonmati, Guotai Wang, Steven Bandula, Caroline M Moore, Mark Emberton, et al. Weakly-supervised convolutional neural networks for multimodal image registration. *Medical image analysis*, 49:1–13, 2018. 1
- [17] Zilong Huang, Xinggong Wang, Jiasi Wang, Wenyu Liu, and Jingdong Wang. Weakly-supervised semantic segmentation network with deep seeded region growing. In *Proceedings of the IEEE Conference on Computer Vision and Pattern Recognition*, pages 7014–7023, 2018. 2
- [18] Muhammad Abdullah Jamal and Guo-Jun Qi. Task agnostic meta-learning for few-shot learning. In *Proceedings of the IEEE/CVF Conference on Computer Vision and Pattern Recognition*, pages 11719–11727, 2019. 2
- [19] Longlong Jing and Yingli Tian. Self-supervised visual feature learning with deep neural networks: A survey. *IEEE transactions on pattern analysis and machine intelligence*, 2020. 1
- [20] Sanghyun Jo and In-Jae Yu. Puzzle-cam: Improved localization via matching partial and full features. *arXiv preprint arXiv:2101.11253*, 2021. 2
- [21] Davood Karimi, Haoran Dou, Simon K Warfield, and Ali Gholipour. Deep learning with noisy labels: Exploring techniques and remedies in medical image analysis. *Medical Image Analysis*, 65:101759, 2020. 3, 5
- [22] Hoel Kervadec, Jose Dolz, Meng Tang, Eric Granger, Yuri Boykov, and Ismail Ben Ayed. Constrained-cnn losses for weakly supervised segmentation. *Medical image analysis*, 54:88–99, 2019. 3
- [23] Hoel Kervadec, Jose Dolz, Shanshan Wang, Eric Granger, and Ismail Ben Ayed. Bounding boxes for weakly supervised segmentation: Global constraints get close to full supervision. In *Medical Imaging with Deep Learning*, pages 365–381. PMLR, 2020. 3
- [24] Anna Khoreva, Rodrigo Benenson, Jan Hosang, Matthias Hein, and Bernt Schiele. Simple does it: Weakly supervised instance and semantic segmentation. In *Proceedings of the IEEE conference on computer vision and pattern recognition*, pages 876–885, 2017. 2
- [25] Diederik P Kingma and Jimmy Ba. Adam: A method for stochastic optimization. *arXiv preprint arXiv:1412.6980*, 2014. 5
- [26] Han Le, Dimitris Samaras, Tahsin Kurc, Rajarsi Gupta, Kenneth Shroyer, and Joel Saltz. Pancreatic cancer detection in whole slide images using noisy label annotations. In *International Conference on Medical Image Computing and Computer-Assisted Intervention*, pages 541–549. Springer, 2021. 1

2019. [3](#)
- [27] Kimin Lee, Sukmin Yun, Kibok Lee, Honglak Lee, Bo Li, and Jinwoo Shin. Robust inference via generative classifiers for handling noisy labels. In *International Conference on Machine Learning*, pages 3763–3772. PMLR, 2019. [3](#)
- [28] Wenhui Lei, Haochen Mei, Zhengwentai Sun, Shan Ye, Ran Gu, Huan Wang, Rui Huang, Shichuan Zhang, Shaoting Zhang, and Guotai Wang. Automatic segmentation of organs-at-risk from head-and-neck ct using separable convolutional neural network with hard-region-weighted loss. *Neurocomputing*, 442:184–199, 2021. [1](#)
- [29] Wenhui Lei, Huan Wang, Ran Gu, Shichuan Zhang, Shaoting Zhang, and Guotai Wang. Deepigeos-v2: deep interactive segmentation of multiple organs from head and neck images with lightweight cnns. In *Large-Scale Annotation of Biomedical Data and Expert Label Synthesis and Hardware Aware Learning for Medical Imaging and Computer Assisted Intervention*, pages 61–69. Springer, 2019. [3](#)
- [30] Wenhui Lei, Wei Xu, Ran Gu, Hao Fu, Shaoting Zhang, Shichuan Zhang, and Guotai Wang. Contrastive learning of relative position regression for one-shot object localization in 3d medical images. In *International Conference on Medical Image Computing and Computer-Assisted Intervention*, pages 155–165. Springer, 2021. [1](#), [2](#), [3](#), [4](#)
- [31] Gen Li, Varun Jampani, Laura Sevilla-Lara, Deqing Sun, Jonghyun Kim, and Joongkyu Kim. Adaptive prototype learning and allocation for few-shot segmentation. In *Proceedings of the IEEE/CVF Conference on Computer Vision and Pattern Recognition*, pages 8334–8343, 2021. [2](#)
- [32] Di Lin, Jifeng Dai, Jiaya Jia, Kaiming He, and Jian Sun. Scribblesup: Scribble-supervised convolutional networks for semantic segmentation. In *Proceedings of the IEEE conference on computer vision and pattern recognition*, pages 3159–3167, 2016. [2](#)
- [33] Damian J Matuszewski and Ida-Maria Sintorn. Minimal annotation training for segmentation of microscopy images. In *2018 IEEE 15th International Symposium on Biomedical Imaging (ISBI 2018)*, pages 387–390. IEEE, 2018. [3](#)
- [34] Fausto Milletari, Nassir Navab, and Seyed-Ahmad Ahmadi. V-net: Fully convolutional neural networks for volumetric medical image segmentation. In *2016 fourth international conference on 3D vision (3DV)*, pages 565–571. IEEE, 2016. [5](#)
- [35] Shaobo Min, Xuejin Chen, Zheng-Jun Zha, Feng Wu, and Yongdong Zhang. A two-stream mutual attention network for semi-supervised biomedical segmentation with noisy labels. In *Proceedings of the AAAI Conference on Artificial Intelligence*, volume 33, pages 4578–4585, 2019. [3](#)
- [36] Tsendsuren Munkhdalai and Hong Yu. Meta networks. In *International Conference on Machine Learning*, pages 2554–2563. PMLR, 2017. [2](#)
- [37] Pavel Ostyakov, Elizaveta Logacheva, Roman Suvorov, Vladimir Aliev, Gleb Sterkin, Oleg Khomenko, and Sergey I Nikolenko. Label denoising with large ensembles of heterogeneous neural networks. In *Proceedings of the European Conference on Computer Vision (ECCV) Workshops*, pages 0–0, 2018. [3](#)
- [38] Cheng Ouyang, Carlo Biffi, Chen Chen, Turkay Kart, Huaqi Qiu, and Daniel Rueckert. Self-supervision with superpixels: Training few-shot medical image segmentation without annotation. In *European Conference on Computer Vision*, pages 762–780. Springer, 2020. [1](#), [2](#), [5](#), [6](#)
- [39] Adam Paszke, Sam Gross, Francisco Massa, Adam Lerer, James Bradbury, Gregory Chanan, Trevor Killeen, Zeming Lin, Natalia Gimelshein, Luca Antiga, et al. Pytorch: An imperative style, high-performance deep learning library. *Advances in neural information processing systems*, 32:8026–8037, 2019. [5](#)
- [40] Hieu H Pham, Tung T Le, Dat Q Tran, Dat T Ngo, and Ha Q Nguyen. Interpreting chest x-rays via cnns that exploit disease dependencies and uncertainty labels. *medRxiv*, page 19013342, 2019. [3](#)
- [41] Martin Rajchl, Matthew CH Lee, Ozan Oktay, Konstantinos Kamnitsas, Jonathan Passerat-Palmbach, Wenjia Bai, Mellisa Damodaram, Mary A Rutherford, Joseph V Hajnal, Bernhard Kainz, et al. Deepcut: Object segmentation from bounding box annotations using convolutional neural networks. *IEEE transactions on medical imaging*, 36(2):674–683, 2016. [3](#)
- [42] Kate Rakelly, Evan Shelhamer, Trevor Darrell, Alexei A Efros, and Sergey Levine. Few-shot segmentation propagation with guided networks. *arXiv preprint arXiv:1806.07373*, 2018. [2](#)
- [43] Mengye Ren, Wenyuan Zeng, Bin Yang, and Raquel Urtasun. Learning to reweight examples for robust deep learning. In *International Conference on Machine Learning*, pages 4334–4343. PMLR, 2018. [3](#)
- [44] Olaf Ronneberger, Philipp Fischer, and Thomas Brox. U-net: Convolutional networks for biomedical image segmentation. In *International Conference on Medical image computing and computer-assisted intervention*, pages 234–241. Springer, 2015. [5](#)
- [45] Abhijit Guha Roy, Shayan Siddiqui, Sebastian Pölsterl, Nassir Navab, and Christian Wachinger. ‘squeeze & excite’guided few-shot segmentation of volumetric images. *Medical image analysis*, 59:101587, 2020. [1](#), [2](#), [6](#)
- [46] Adam Santoro, Sergey Bartunov, Matthew Botvinick, Daan Wierstra, and Timothy Lillicrap. One-shot learning with memory-augmented neural networks. *arXiv preprint arXiv:1605.06065*, 2016. [2](#)
- [47] Amirreza Shaban, Shray Bansal, Zhen Liu, Irfan Essa, and Byron Boots. One-shot learning for semantic segmentation. *arXiv preprint arXiv:1709.03410*, 2017. [1](#), [2](#)
- [48] Jialin Shi and Ji Wu. Distilling effective supervision for robust medical image segmentation with noisy labels. *arXiv preprint arXiv:2106.11099*, 2021. [3](#)
- [49] Jake Snell, Kevin Swersky, and Richard S Zemel. Prototypical networks for few-shot learning. *arXiv preprint arXiv:1703.05175*, 2017. [2](#)
- [50] Sainbayar Sukhbaatar and Rob Fergus. Learning from noisy labels with deep neural networks. *arXiv preprint arXiv:1406.2080*, 2(3):4, 2014. [3](#)
- [51] Flood Sung, Yongxin Yang, Li Zhang, Tao Xiang, Philip HS Torr, and Timothy M Hospedales. Learning to compare: Relation network for few-shot learning. In *Proceedings of the IEEE conference on computer vision and pattern recognition*, pages 1199–1208, 2018. [2](#)
- [52] Nima Tajbakhsh, Laura Jeyaseelan, Qian Li, Jeffrey N Chi-

- ang, Zhihao Wu, and Xiaowei Ding. Embracing imperfect datasets: A review of deep learning solutions for medical image segmentation. *Medical Image Analysis*, 63:101693, 2020. 2
- [53] Hao Tang, Xingwei Liu, Shanlin Sun, Xiangyi Yan, and Xiaohui Xie. Recurrent mask refinement for few-shot medical image segmentation. In *Proceedings of the IEEE/CVF International Conference on Computer Vision*, pages 3918–3928, 2021. 2
- [54] Oriol Vinyals, Charles Blundell, Timothy Lillicrap, Daan Wierstra, et al. Matching networks for one shot learning. *Advances in neural information processing systems*, 29:3630–3638, 2016. 2
- [55] Guotai Wang, Wenqi Li, Sébastien Ourselin, and Tom Vercauteren. Automatic brain tumor segmentation using cascaded anisotropic convolutional neural networks. In *International MICCAI brainlesion workshop*, pages 178–190. Springer, 2017. 1
- [56] Guotai Wang, Xinglong Liu, Chaoping Li, Zhiyong Xu, Jiugen Ruan, Haifeng Zhu, Tao Meng, Kang Li, Ning Huang, and Shaoting Zhang. A noise-robust framework for automatic segmentation of covid-19 pneumonia lesions from ct images. *IEEE Transactions on Medical Imaging*, 39(8):2653–2663, 2020. 3
- [57] Guotai Wang, Maria A Zuluaga, Wenqi Li, Rosalind Pratt, Premal A Patel, Michael Aertsen, Tom Doel, Anna L David, Jan Deprest, Sébastien Ourselin, et al. Deepigeos: a deep interactive geodesic framework for medical image segmentation. *IEEE transactions on pattern analysis and machine intelligence*, 41(7):1559–1572, 2018. 3, 5
- [58] Kaixin Wang, Jun Hao Liew, Yingtian Zou, Daquan Zhou, and Jiashi Feng. Panet: Few-shot image semantic segmentation with prototype alignment. In *Proceedings of the IEEE/CVF International Conference on Computer Vision*, pages 9197–9206, 2019. 1, 2
- [59] Ke Yan, Jinzheng Cai, Dakai Jin, Shun Miao, Adam P Harrison, Dazhou Guo, Youbao Tang, Jing Xiao, Jingjing Lu, and Le Lu. Self-supervised learning of pixel-wise anatomical embeddings in radiological images. *arXiv preprint arXiv:2012.02383*, 2020. 2, 3
- [60] Qingsong Yao, Quan Quan, Li Xiao, and S Kevin Zhou. One-shot medical landmark detection. *arXiv preprint arXiv:2103.04527*, 2021. 2, 3
- [61] Rumeng Yi, Yaping Huang, Qingji Guan, Mengyang Pu, and Runsheng Zhang. Learning from pixel-level label noise: A new perspective for semi-supervised semantic segmentation. *arXiv preprint arXiv:2103.14242*, 2021. 5
- [62] Lequan Yu, Shujun Wang, Xiaomeng Li, Chi-Wing Fu, and Pheng-Ann Heng. Uncertainty-aware self-ensembling model for semi-supervised 3d left atrium segmentation. In *International Conference on Medical Image Computing and Computer-Assisted Intervention*, pages 605–613. Springer, 2019. 3
- [63] Jingyang Zhang, Guotai Wang, Hongzhi Xie, Shuyang Zhang, Ning Huang, Shaoting Zhang, and Lixu Gu. Weakly supervised vessel segmentation in x-ray angiograms by self-paced learning from noisy labels with suggestive annotation. *Neurocomputing*, 417:114–127, 2020. 3
- [64] Xiaolin Zhang, Yunchao Wei, Yi Yang, and Thomas S Huang. Sg-one: Similarity guidance network for one-shot semantic segmentation. *IEEE transactions on cybernetics*, 50(9):3855–3865, 2020. 1, 2
- [65] Yikai Zhang, Songzhu Zheng, Pengxiang Wu, Mayank Goswami, and Chao Chen. Learning with feature-dependent label noise: A progressive approach. *arXiv preprint arXiv:2103.07756*, 2021. 3
- [66] Amy Zhao, Guha Balakrishnan, Fredo Durand, John V Guttag, and Adrian V Dalca. Data augmentation using learned transformations for one-shot medical image segmentation. In *Proceedings of the IEEE/CVF Conference on Computer Vision and Pattern Recognition*, pages 8543–8553, 2019. 1, 5, 6
- [67] Yaoyao Zhong, Weihong Deng, Mei Wang, Jiani Hu, Jianteng Peng, Xunqiang Tao, and Yaohai Huang. Unequal-training for deep face recognition with long-tailed noisy data. In *Proceedings of the IEEE/CVF Conference on Computer Vision and Pattern Recognition*, pages 7812–7821, 2019. 3
- [68] Bolei Zhou, Aditya Khosla, Agata Lapedriza, Aude Oliva, and Antonio Torralba. Learning deep features for discriminative localization. In *Proceedings of the IEEE conference on computer vision and pattern recognition*, pages 2921–2929, 2016. 2
- [69] Yi Zhou, Xiaodong He, Lei Huang, Li Liu, Fan Zhu, Shanshan Cui, and Ling Shao. Collaborative learning of semi-supervised segmentation and classification for medical images. In *Proceedings of the IEEE/CVF Conference on Computer Vision and Pattern Recognition*, pages 2079–2088, 2019. 1